Experimental and Analytical Behaviour of Prefabricated Pretensioned Moment-Resistant Column-to-Column Spliced Joints

Yufeng Jiao*

Engineering College, Sanda University, Shanghai 201209, China;

* Correspondence: yufengjiao@sandau.edu.cn

Abstract: To facilitate the rapid construction of steel or steel-concrete structures, a new type of spliced joint, called a prefabricated pretensioned moment-resistant joint, was designed to splice H-shaped steel columns. Two supporting plates, sustained by two stiffened ribs, were welded near the end of the column, which could be prefabricated in a factory. Two segments of the H-shaped steel column were linked by longitudinal high-strength bolts (LHSBs), which were pretensioned to provide precompression in the milled flange of the column. In this paper, reversed cyclic loading tests were conducted on three specimens of this innovative joint to investigate its failure modes and load-bearing capacity influencing factors. A finite element(FE) model of the tested specimens was developed, and the results obtained from the FE modelling were verified against those from the test results. The results indicate that the LHSBs have such a remarkable connection ability that the load-bearing capacity is strong even if buckling deformation occurs in the flange of the column. The joint was damaged due to the loosening of the LHSBs accompanied by the separation of the two flanges of the column. Parametric studies were conducted to investigate the influence of steel strength, bolt pretension force, flange bolt diameter, etc, on the behaviour of the connection. The results show that the ratio β and pretension of the LHSB have a great influence on the joint performance. When a pretension of 0.8P is applied(P is pretension of high-strength bolt), the ultimate moment can be reduced by 15.8%; when a pretension of 0.6P is applied, the ultimate moment can be reduced by 24.5%. When the ratio β large, the flange at the column splicing joint is prone to local instability, thus accelerating the failure of the joint.

Keywords: prefabricated pretensioned moment-resistant connection; column-to-column joint; cyclic experiment; long longitudinal high-strength bolt; parametric study

1. Introduction

Steel structures are easily adaptable to modularization, industrial production and on-site installation; therefore, steel structures have become the most suitable structure type for the development of prefabricated structures, following the green building definition proposed in the Assessment Standard for Green Building[1]. In on-site constructed fabricated steel structures, the joint connection is particularly important, and the joint structure design is greatly affected by the assembly construction. Due to the specific characteristics of a fabricated steel structure, the joint of the frame is particularly important. The connection performance directly affects the feasibility of the structure assembly and the seismic performance of the whole fabricated structure. At present, research of fabricated steel frame joints at home and abroad is mostly focused on low-rise buildings[2-5], and most of these studies consider a special fabricated structural system. CHEN Yueshi et al[6] proposed a new type of floor-by-floor assembled steel braced structure for prefabricated buildings; this structure is composed of a highly standardized H-shaped steel beam, square steel pipe column and flat steel flexible support. It is easy to construct on site because the beam is full-length and the column is connected at the beam-column joint. The test of a three-story frame showed that the frame system exhibits excellent seismic performance and post-earthquake resilience. Zhang Yanxia et al[7] proposed a prestressed fabricated steel frame system with the recoverable function of a web friction damper, and in this frame, the prestressed fabricated steel frame connection is realized by setting a prestressed steel strand and energy-dissipating angle iron. At present, there are few studies on prefabricated high-rise buildings. LIU X.C. et al[8-9] studied a modularized prefabricated multi-rise and high-rise steel structure, composed of a singleangle truss beam and square pipe column. The truss beam is welded onto the column base and the vertical connecting plate, which forms one module. Two pieces of a single-angle truss beam are spliced by the bolt at the intersection joint.

In the study of the connection of fabricated steel structures, research has focused on beam-column joints. In contrast, much less attention has been paid to column splices, which are important for the long-term performance of individual columns. As the main part of the column, the splices are located at a convenient distance for erection and construction above the floor beam level and have to be designed to connect segments, to transfer force and moments between the connected member parts and to maintain the continuity of stiffness through the splice to safeguard the robustness of the structure.

The research on column joints mainly focuses on the stability design and influence of the splice form on the load carrying capacity and buckling of the columns. H.H. Snijder[10] conducted full-scale experimental tests on three different column splices to analyse the influence of end plate splices on the bearing capacity and identify requirements for column splices with respect to

stability. Based on their tests, the strength and stiffness criteria of the spliced column are obtained, and it is found that a spliced column connected by an end plate has an adverse effect on the buckling load of the column. Therefore, they suggested that the strength design of column splices be performed under an axial force and a second-order bending moment and the corresponding shear force. Therefore, they also give the formula of the initial rotational stiffness of the column, which plays an important role in later research. Ana M. Girão Coelho[11] further extended this work by examining the buckling behaviour of an axially loaded framed spliced steel column. After implementing parametric studies to study factors such as the splice location and rotational stiffness, change in the column section serial size and column end- restraint stiffness coefficients, simple relationships were developed for use as a basic stiffness design criterion for column splices in non-sway frames. Pedro D. Simão [12] studied the influence of splicing form on column buckling. The parameters studied included the splicing rotational stiffness, restraint coefficient of the column end, splicing position and area ratio of the upper and lower column segments. Based on the energy equation, by defining the end consolidation coefficient C and combining the research results on the parameter influences, the regression equation was derived to obtain the critical buckling load of the column. Some researchers have studied the seismic demand on column splices involving uncertainties in both ground motion characteristics and structural parameters. Shen et al. [13] studied the seismic demand on column splices in special moment frames to evaluate whether the seismic design provisions as set forth by AISC 341[14] requiring CJP groove welds at column splices are justified or unnecessarily conservative. However, Bulent Akbas[15] utilized a neural network(NN) model to estimate the seismic demands on column splices in low-, medium-, and highrise steel moment frames. Then, Bulent Akbas[16] conducted a comprehensive nonlinear analytic investigation to evaluate the effect of various span lengths on the seismic demand on column splices in steel moment-resisting frames. The results indicate that the structural response was sensitive to the span length and variable span length.

Regarding the splicing of columns, the transmission of pressure depends on the contact between splices. Many analysis results are determined by assuming full section contact. However, according to actual engineering and test results, there will be a separation phenomenon at the splice during the stressing of the columns. C. C.baniotopoulos[17]used variational inequality and quadratic optimization methods to study the incomplete contact problem of a bolted column end plate joint for the first time. Furthermore, J. Lindner[18] studied contact splices by examining the influence of the initial defects on the buckling behaviour. Because of the eccentricity of the column section caused by initial imperfections, the contact area was gradually reduced. The author considered this influence in the testing and included it in the finite element analysis to propose an adjusted buckling curve for columns with contact splices at the mid-height.

Because of the different cross-sectional forms of columns, there is no uniform joint shape and research on column splice types is very limited. At present, welding is often used for column splicing in engineering projects. However, the performance of welded joints is not satisfactory. Post-earthquake[19-20], many brittle fractures were found at several welding heat-affected zones of the welded beam-column or column-column splicing joint. Kimberly Stillmakera et al[21] studied the seismic response of 4- and 20-story moment frames with welded column splice fractures and provided a general commentary regarding the retro-fitting of pre-Northridge SMRF buildings. Carmine Galasso et al[22] assessed the seismic demands and capacities of welded column splice (WCS) connections in steel moment frames and conducted probabilistic risk analysis of splice fracture within a framework based on performance-based earthquake engineering (PBEE). The research mentioned above mainly focused on the welded column splice fracturing that can cause severe seismic damage. If columns are not welded together by forming a a splice with a uniform strength, too many bolts will be needed. In engineering projects, bolted-flange connections are widely used in steel tubular structures[23-24]. These spliced joints require a large amount of welding work on site, or more bolts are used, which is not conducive to reducing the construction cost of fabricated steel structures. Liu[25] proposed a new type of bolted connection that can be used to connect trusses to columns and columns to columns on site in modularized prefabricated multi-rise and high-rise steel structures. However, these joints are only suitable for rectangular hollow section (RHS) columns in prefabricated multi-high-rise steel structures, not for common I-shaped columns.

The research mentioned above focuses on the structural behaviour of common splice type, which has been widely used due to its favourable performance in steel frame structures. However, the distinctive disadvantages of column splices are complicated construction and difficult quality control on site, eventually increasing field erection costs. There has been no study on splice detail improvement, especially on the details facilitating simple assembly and rapid construction for large projects. In particular, a feasible bolted connection between columns has not yet been proposed and its bearing capacity and seismic performance need further study. Consequently, a prefabricated pretensioned moment-resistant spliced joint is proposed.

Columns are usually spliced at one-quarter of the way up a column from a particular storey. Two supporting plates, sustained by two stiffened ribs, are welded near the end of the column, which can be prefabricated in a factory. The distinguishing feature of

the improved joint detail is that two segments of the I-steel column are linked by four longitudinal high-strength bolts (Grade 12.9), which are pretensioned to provide precompression for the milled flange of the column, as shown in Figure 1. The friction posed by the precompression mentioned above can resist shear force and the variation in the precompression can resist moment. The moment-resistant capacity, produced by applying a high pretension to the longitudinal high-strength bolts, ensures the continuity of the bending stiffness and strength of the members. The shear force can be resisted through the high-strength bolts at the web of the column and can be calculated according to the internal force at the splice position.

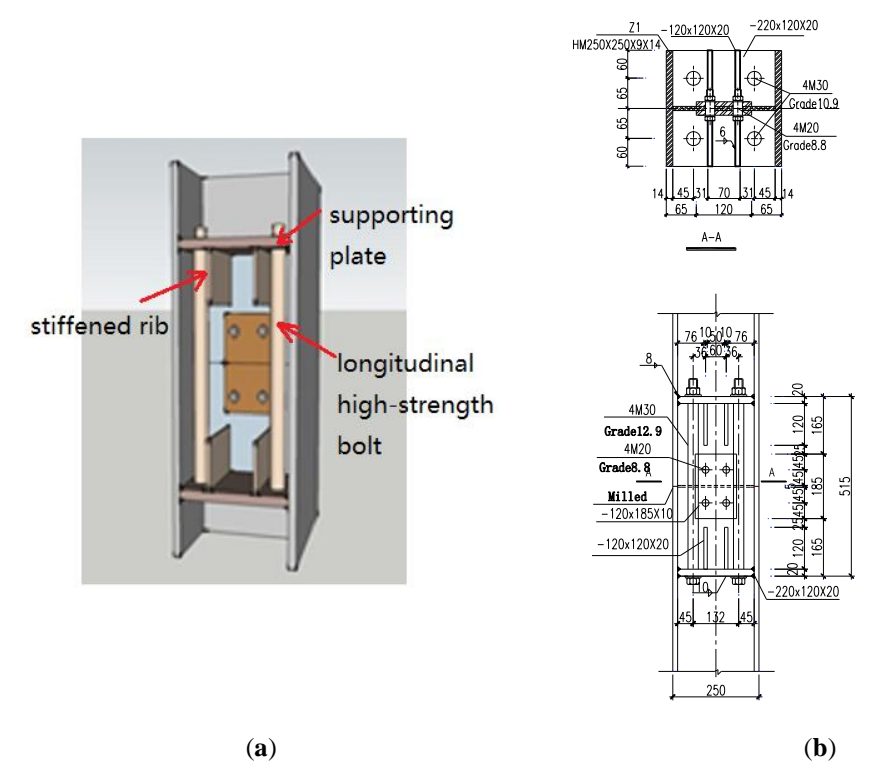


Figure 1. Details of the pretensioned moment-resistant spliced joint; (a) Three-dimensional diagram; (b) Detail drawing

To further investigate the proposed splice joint behaviour, three full-scale specimens were subjected to reversed cyclic loading tests, which were used as the calibration basis for the numerical studies. Then cyclic loading finite element simulation calculations were carried out to analyse the stress distribution, yield area and failure mode of the joint components. Compared with the test results, the validity and feasibility of the finite element model and the accuracy of the joint design formula are verified. On this basis, the finite element models for five series and 50 joints are established by changing the joint parameters, and the main influencing factors of the initial stiffness and ultimate bearing capacity of the joints areanalysed, which provides the basis for a more accurate evaluation of the overall failure mode of the structure and the engineering application of the joints.

2. Experimental Programme

2.1. Test specimen design

The component size of the joint can be determined by the internal force at the column. Specifically, the column web at a splice is subjected to axial compression and a shear force. Hence, the number of high-strength bolts is calculated by eq. (1). The longitudinal high-strength bolts (LHSBs) alternate between tension and compression states when the column undergoes a horizontal load and the column section centre is taken as the rotational centre. As a result, the diameter of the longitudinal bolts can be designed by using eq. (2). The thickness of splice flange plates is determined by eq. (3)

$$n_{wc} \ge \sqrt{\left(\frac{A_w}{A}N\right)^2 + V^2} / N_v^{bH} \tag{1}$$

where n_{wc} is the number of web bolts. Aw and A are the column web area and sectional area, respectively. N is the axial compression of the column and V is the shear force at the splice. N_w^{bH} is the shear capacity of the bolt.

$$\frac{M_j}{h} \le 0.8P \tag{2}$$

where Mj is the bending moment at the splice and h is the central distance between two LHSBs. P is the bolt pretension load. Because of the relationship between the bolt diameter and pretension load, equation (2) could be used to choose the bolt dimension.

$$t \ge \sqrt{\frac{5M_{\text{max}}}{f}} \tag{3}$$

where Mmax is the maximum moment of the splice flange plate per unit width and f is the design value of the strength. Because the supporting plate is welded at three sides, it can be considered a plate with three sides clamped and the other free, and uniform compressive stress is applied. With this boundary condition the maximum moment could be obtained.

Three test specimens (C1-1, C1-2, C1-3) are designed for the test, and the detailed structure and geometric dimensions of the three test pieces are the same, as shown in Figure 2. All specimens were fabricated using Grade Q345B steel with a minimum yield strength of 345 MPa. The cross section size of the beam and column was $HN250 \times 250 \times 9 \times 14$, and an M20 friction type high-strength bolt of Grade 8.8 was used for web splicing. The supporting plates were linked by two LHSBs with Grade 10.9, which were non-standard manufactured bolts. The shear friction coefficients of the high-strength bolts used in the test were all 0.4. The web splicing bolts were tightened to a 125kN pretention force, while the LHSBs were tightened to a 355kN pretention force, following the specification GB50017-2017 [26]. Before the test, three tension test samples were extracted from the column flange with a thickness of 14mm. Table 1 lists the mechanical properties of the steel profiles.

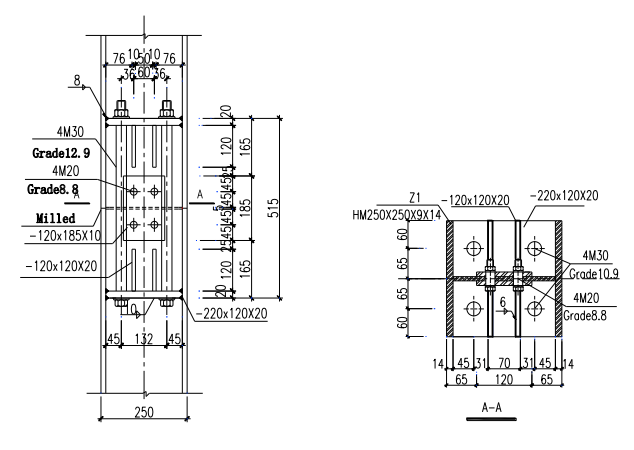


Figure 2. Details of the specimens

Table 1. Results of the coupon test

Specimen	Specimen Elastic modu- lus/MPa		Tensile strength fu(MPa)	Elongation (%)	Yield ratio fy/fu	
C1-1	1.98×10 ⁵	384.22	483.23	22.1	0.79	
C1-2	1.89×10^{5}	359.14	488.36	21.3	0.74	
C1-3	2.02×10^{5}	391.68	497.57	18.2	0.78	

2.2. Test specimen design

Figure 3 illustrates the test setup and the locations of the displacement transducers and strain gauges. The test was completed in the Structure Laboratory of Tongji University. The bottom of the column was fixed to the rigid ground groove in the laboratory with M56 bolts. To strengthen the bottom of the column, limit beams were used on both sides of the column. The left limiting beam was jacked tightly with the reaction frame, and the right limiting beam was connected to the reaction frame by a steel pipe.

The horizontal loading point was located one metre away from the spliced point. Two steel plates were welded at the flanges of the steel column at the loading point. Thus, the column was connected to the jack by four M30 bolts. A 50t hydraulic jack was linked to the reaction frame and horizontal cyclic loading was applied. A hydraulic jack was set on the column top; the upper end of the jack was fixed on the side reaction frame, and the lower end was connected to the test member with a ball-and-hinge device to exert 600 kN of axial pressure on the column top. To apply the axial force on the top of the column successfully, a $500 \times 450 \times 30$ steel plate was welded on the top of the column, and the stiffening plate was welded on the bottom of the steel plate, as shown in Figure 3 (b).

The specimens were equipped with displacement transducers and strain gauges, as shown in Figure 3 (b)~(c). The displacement meters D1, D2 and D3 were horizontally arranged on the right side of the column to measure the lateral displacement and relative angle of the splicing column. The displacement meter D4 was arranged vertically at the joint to measure the vertical displacement of the steel column under axial pressure. The displacement meters D5 and D6 were arranged diagonally across the splicing node region to measure the shear deformation at the panel zone. Unidirectional strain gauges were arranged on the column flange and LHSB. To investigate the complex stress state of the supporting plate and stiffener, as well as the stress development and elastic-plastic deformation in this area, three-direction strain gauges were also arranged at these two components.

The numbering scheme in Figure 3 is as follows: S1, S2, etc, are the numbers of the unidirectional strain gauges. In the strain gauge layout of the LHSB, the brackets are numbered on the right side. T1 is the three-direction strain gauge of the upper supporting plate and T19 in the bracket indicates another side of it. T2 is the bottom supporting plate and T20 indicates another side. The numbering scheme of the stiffened rib is consistent with that of the supporting plate.



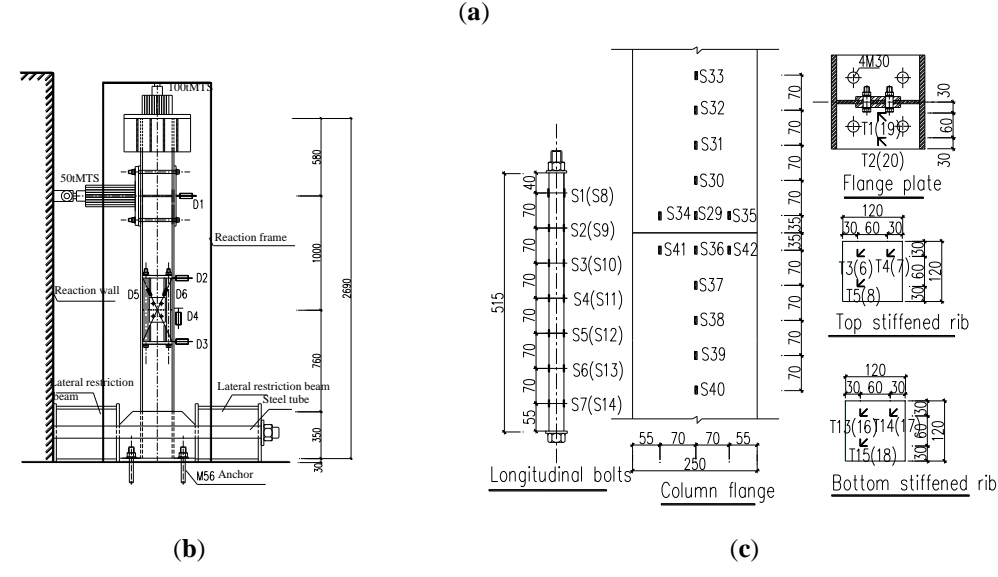


Figure 3. Layout of the specimen (a) Test set-up; (b) Schematic view; (c) Measurement points

2.3. Loading protocol

One preload was conducted before the formal test. One cycle of the reciprocating load cycle was exerted with a preload of 3 kN. Displacement control was adopted for test loading. The specific loading methods are as follows: 1) apply the vertical load on the top of the column to the axial force of approximately 600 kN (the actual axial compression ratio of the corresponding column is n = 0.24), and keep it constant throughout the test process; 2) apply the repeated horizontal load 1 m from the spliced point, and add the load once to obtain each displacement value. The displacement value of each stage of loading was determined according to the displacement at the actuator, starting from 5 mm and increasing by 5 mm at each stage, until the test specimen lost the bearing capacity and could not be loaded.

3. Test Results and Discussion

3.1 Failure mode

The failure modes of the three specimens were basically the same, but during the test of the C1-3 specimen, the hinged end of the jack on the top of the column was not firmly fixed to the vertical reaction frame, and the connecting bolts loosened. When the horizontal load of C1-3 increased, the lateral displacement was larger than those of C1-1 and C1-2. Therefore, this paper focuses on the failure modes of C1-1 and C1-2.

In the elastic stage, there was no sound during the loading process, and the deformation of the joint was very small. When the horizontal load approached approximately $P = \pm 160$ kN, some quiet noise could be heard, and the bolts at the web splice plate became slightly loose; when the positive load reached 190 kN, the web splice plate slipped, and the flange at the end of the lower column section partially buckled; when the reverse load reached a horizontal displacement of approximately 30 mm, the flange at the end of the two column sections buckled, and the deformation was semi-wavy. At this time, there was no obvious deformation of the supporting plate and the stiffened rib, but the displacement of the column end at the loading point increased, the LHSB loosened, and the column tilted, as shown in Figure 4. At this moment, the web splice plate slid and rotated, and the bolt of the web also slipped. Finally, the specimen was damaged due to the loss of pretension of the LHSBs, accompanied by buckling of the upper and lower flanges of the column.

The reason for the buckling of the column flange at the spliced joint is that the flange of the two column sections was milled during processing. Therefore, when the two flanges were butted, they were connected by milling. After the pretension was applied to the longitudinal high-strength bolt, the two flanges were connected tightly. Therefore, when the horizontal load was applied to the upper column section, the connection of the two columns depended on the LHSB. However, with increasing load, the effect of the LHSB gradually weakened, resulting in the flanges of the joint zone gradually staggering, so that they could no longer maintain the vertical state. When the load continued to increase, the shear resistance of the joint was weakened and flange buckling occurred at the spliced joint.



Figure 4. Failure mode of specimens

3.2 Hysteresis curve

A hysteresis curve can comprehensively reflect the elastic and inelastic properties, bearing capacity, stiffness and other properties of the specimen. Although the hysteresis curve mainly reflects the ductility performance of the joint, there is no ductility requirement in the performance of the steel column splicing joint. However, the hysteresis curve can be used as a reference for the ultimate bearing capacity of the studied joint under cyclic loading, and it can also be used to investigate whether the stiffness of the joint is continuous. Therefore, the load-displacement hysteresis curves of the loading points of the three specimens are given, as shown in Figure 5.

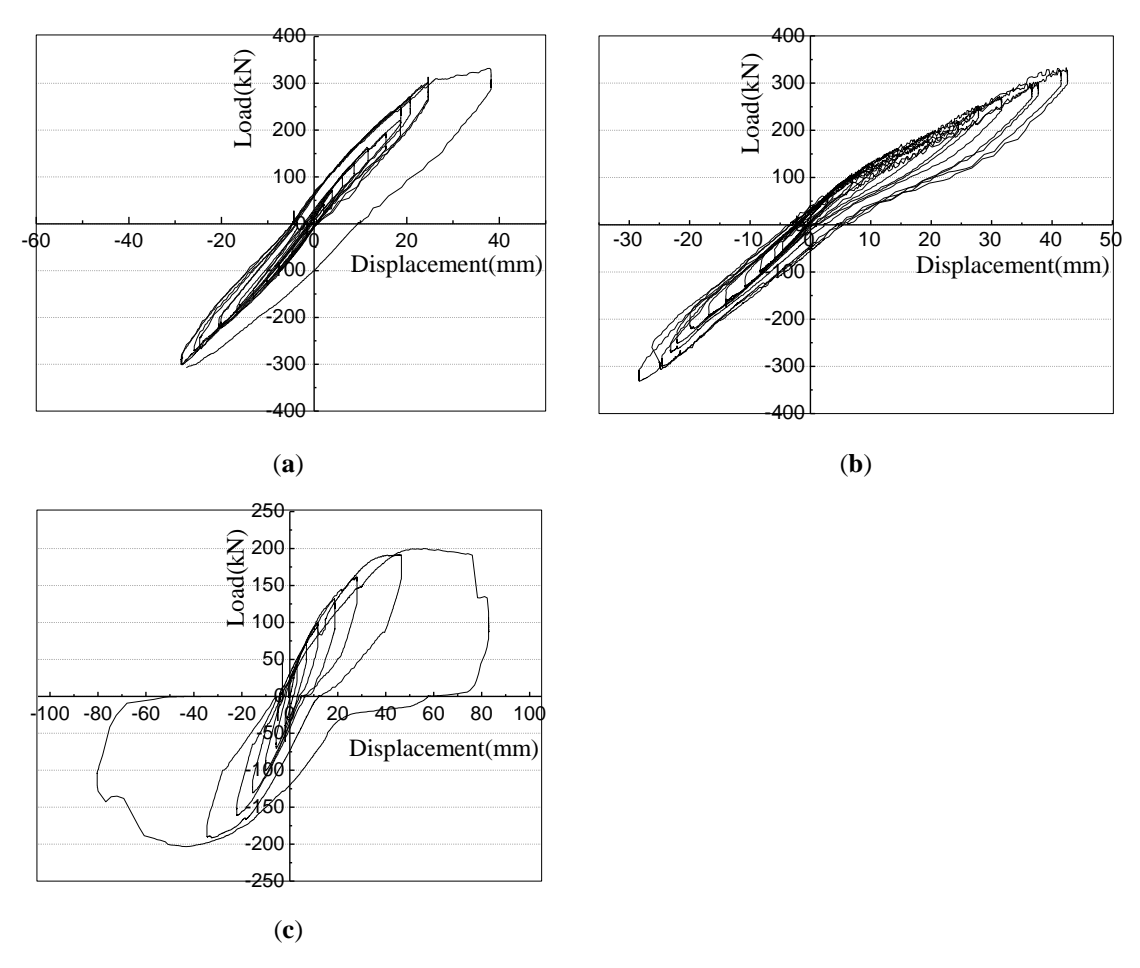


Figure 5. Load-displacement curve at the D1 measurement point; (a) C1-1; (b) C1-2; (c) C1-3

Figure 5 shows that the hysteresis curves of specimens C1-1 and C1-2 are similar, with obvious spindle shapes and smooth curves. Specimen C1-3 is different from C1-1 and C1-2 because the jack at the top of the column was not fixed to the reaction frame tightly, leading to the lateral displacement reaching 80 mm, doubling that of the first two specimens. The estimation and analysis of the stress of the frame column under the cyclic load suggests that the hysteresis curves of C1-1 and C1-2 are closer to the estimated results, so the analysis of the test results are based on these two specimens.

From Figure 5(a)-(b), it can be seen that under the horizontal cyclic load, the maximum displacement of the column is 40 mm, and the ultimate load reaches 330 kN. The envelope area of the curve is small, and the energy consumption is small. There is no plastic hinge in the column joint, and the joint stiffness is large. The joint can resist and transfer the moment, shear and other internal forces to ensure the continuity of the bearing capacity of the column. Overall, the new column-to-column spliced joint has a large bearing capacity and good deformation capacity.

3.3 Strain analysis of LHSB

As an important connection component, LHSBs guarantee the connection of two column segments. As a result, it is necessary to study the strain distribution in these systems. Figure 6 demonstrates the load-strain relationship of every measured point. The figure shows that symmetry does not exist on the strain distribution of the two LHSBs. Figure 6(a) shows that the screw strain on the left side was small. When the joint reached the failure load, the screw strain remained small. The maximum strain, which was 165.3×10^{-6} , occurred at measuring point S1. The strain distribution of the screw on the left side is not uneven, and the distribution close to the upper flange plate changes greatly. Figure 6(b) shows that the maximum strain at measuring point S8, which corresponds to measuring point S1 of the left bolt, can reach -963.2×10⁻⁶. The strain values of the 7 measuring points on the right side tend to be uniform.

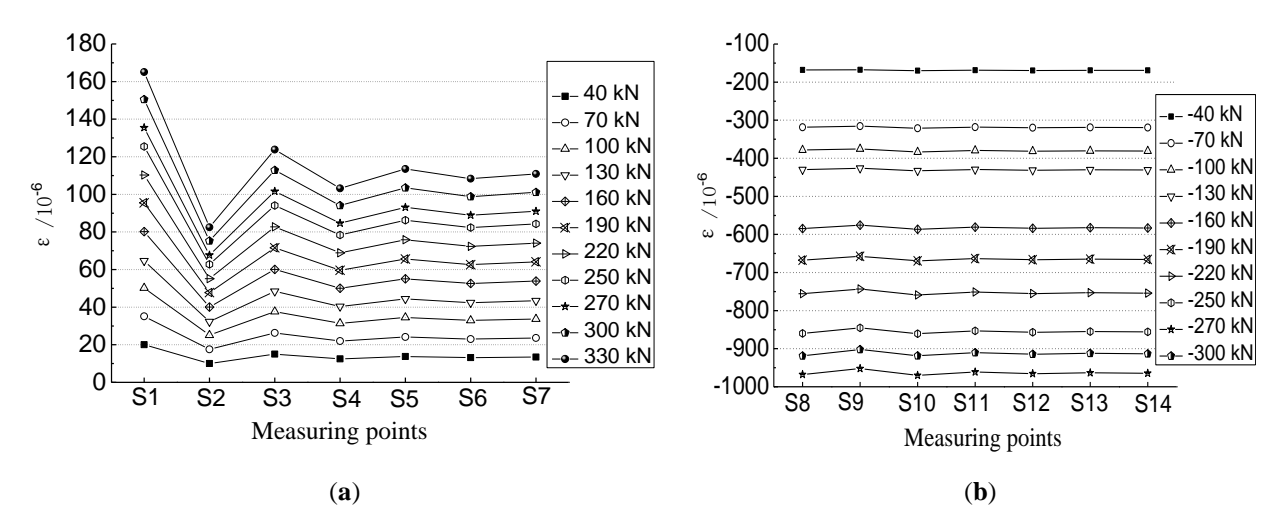


Figure 6. Strain distribution of the LHSBs (a) Left bolt; (b) Right bolt

Unlike conventional high-strength bolt connections, in this column-to-column connection, LHSB was preloaded to link the two column segments. The LHSB was designed as a friction-type bolt. Under the action of a horizontal cyclic load, the horizontal shear force was transmitted by friction force. When the load was small, the screw strain distribution of the LHSB was uniform. With increasing load, the nut became loose, and the friction force at the contact with the supporting plate gradually disappeared. The flanges of the two columns were no longer in close contact. Therefore, the LHSB changed from a friction-type bolt to a pressure-type bolt, and the pressure between the bolt and the hole wall of the supporting plate also transferred a small part of the shear force so that the joint could continue to bear the load.

At this time, the screw alternated between the states of tension and compression. However, due to the large diameter and high strength of this component, there was inevitably a stress change lag phenomenon, which made the strains of the left and right bolts change in differently. In addition, the hole wall at the hole opening of the supporting plate was the stress concentration position, and the screw was in close contact with the supporting plate at the hole. The stress redistribution after the stress concentration of the supporting plate also affected the screw strain.

3.4 Load-stress relationship of the column flange

The stress changes in the column flanges of the three specimens were similar, so specimen C1-1 is taken as an example here. Figure 7 (a) and (b) demonstrate the load-stress curve under a pushing load and pulling load of the upper segment column flange from the right side.

Figure 7 (a) shows that a larger stress arises near the column flange splice zone under push loading. Accordingly, the flange of this area buckled first, leading to failure of the alignment between two segments. In the pushing loading, the stress at measuring point S35 near the splicing point is high, up to 253.99 MPa, and the stress gradually decreases with the distance from the splicing point. These change characteristics are consistent with the test phenomenon. During the test, it was observed that the yield deformation of the flange first occurred near the splicing point. As the longitudinal high-strength bolt was pretensioned, the contact action between the flanges of the two-segment column was strong. Therefore, when the column joint was subjected to the cyclic load, the flange was compressed, and local buckling occurred first, so it was no longer in the contact state. Under reverse loading, only measuring points S34 and S35 near the flange splicing point were in the compression state, with a maximum compressive stress of 90.22 MPa. However, with the increase in load, the test points far away from the joint gradually changed from exhibiting compression to exhibiting tension.

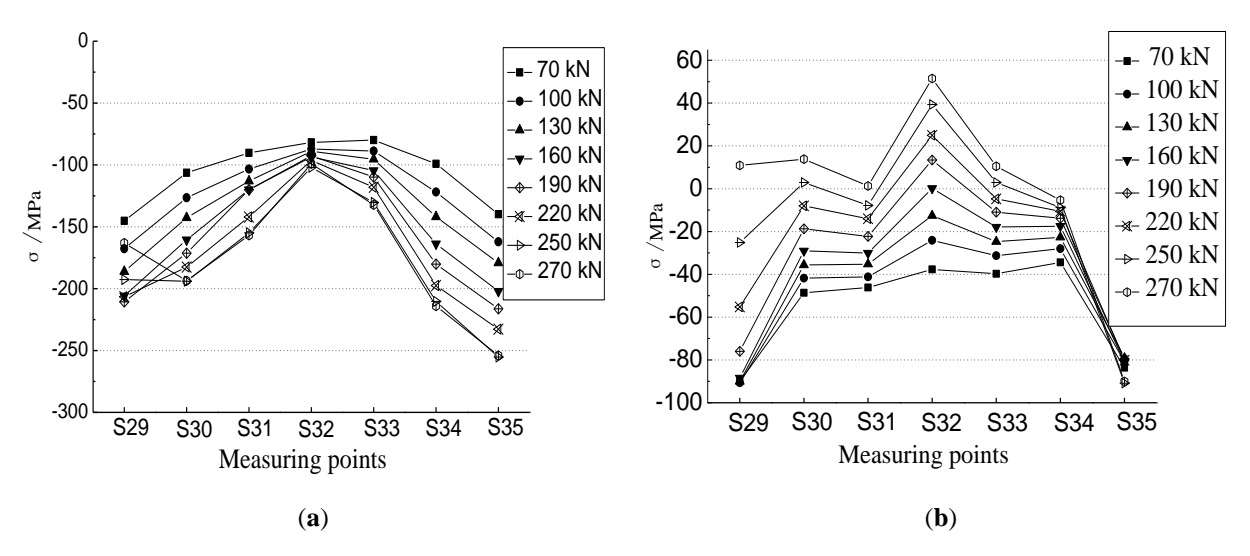


Figure 7. Stress distribution of the top flange of the column (a) Pushing loading; (b) Pulling loading

Figure 8 demonstrates the stress curve of the flange of the bottom segment. It can be seen from the figure that measuring point S36 reaches the yield state first, and the external load is 220 kN. By comparing those results with the flange stress of the upper segment in Figure 7, it can be seen that the variation characteristics of the flange stress of the bottom section of the column are similar to that of the upper section. That is, the stress near the splicing area is high, but the stress values of the two flanges are different. The main reason for this difference is that after the vertical axial force was applied, the column was in the compression state, and the loading point was in the upper column, so the upper segment of the column was in the cyclically alternating tension-compression state. For the bottom segment of the column, the end of the column was consolidated in the laboratory floor groove, and it remained in the state of compression, so the increase rate of the compressive stress is much faster than that of the upper column, which made the flange plate at the joint buckle first, causing severe wave-shaped deformation, resulting in staggering of the upper and lower flanges and the loss of contact action.

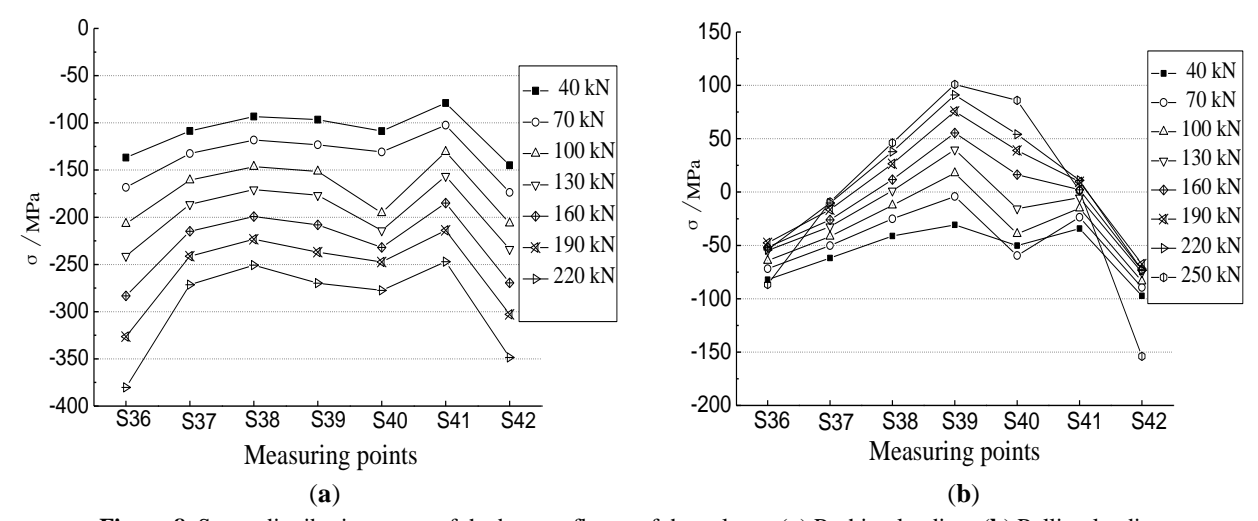


Figure 8. Stress distribution curve of the bottom flange of the column (a) Pushing loading; (b) Pulling loading

3.5 Load-stress relationship of the column flange

Figure 9 shows the load-strain curves of the typical measuring points of the upper column of specimen C1-1, including measuring points S34 and S35 near the splicing point and S31 far from the splicing point.

Comparing Figure 9 (a) and Figure 9 (b), it can be seen that the strain increases slowly at the initial loading stage, and when the load reaches approximately P=+330 kN, the flange strain at the splicing point of the steel column increases sharply. The ultimate strain of measuring point S35 is 5005.3×10⁻⁶, which is higher than that of measuring point S34. Because of the symmetry of the positions of the two measuring points, the limit strain is theoretically equal. However, due to the slight eccentricity of the vertical load, the first yield zone forms near measuring point S35. Combined with the test phenomenon, the column flange deformed when the load was 190 kN. Nevertheless, with the high connection performance of the pretensioned LHSB, the joint continues

to bear a load. From Figure (c), it can be seen that the strain of measuring point S31 far from the flange joint is smaller, and the maximum value is 762.3×10^{-6} , which is 84.8% less than that of measuring point S35. At the end of the test, the stress near this area has not reached the yield point.

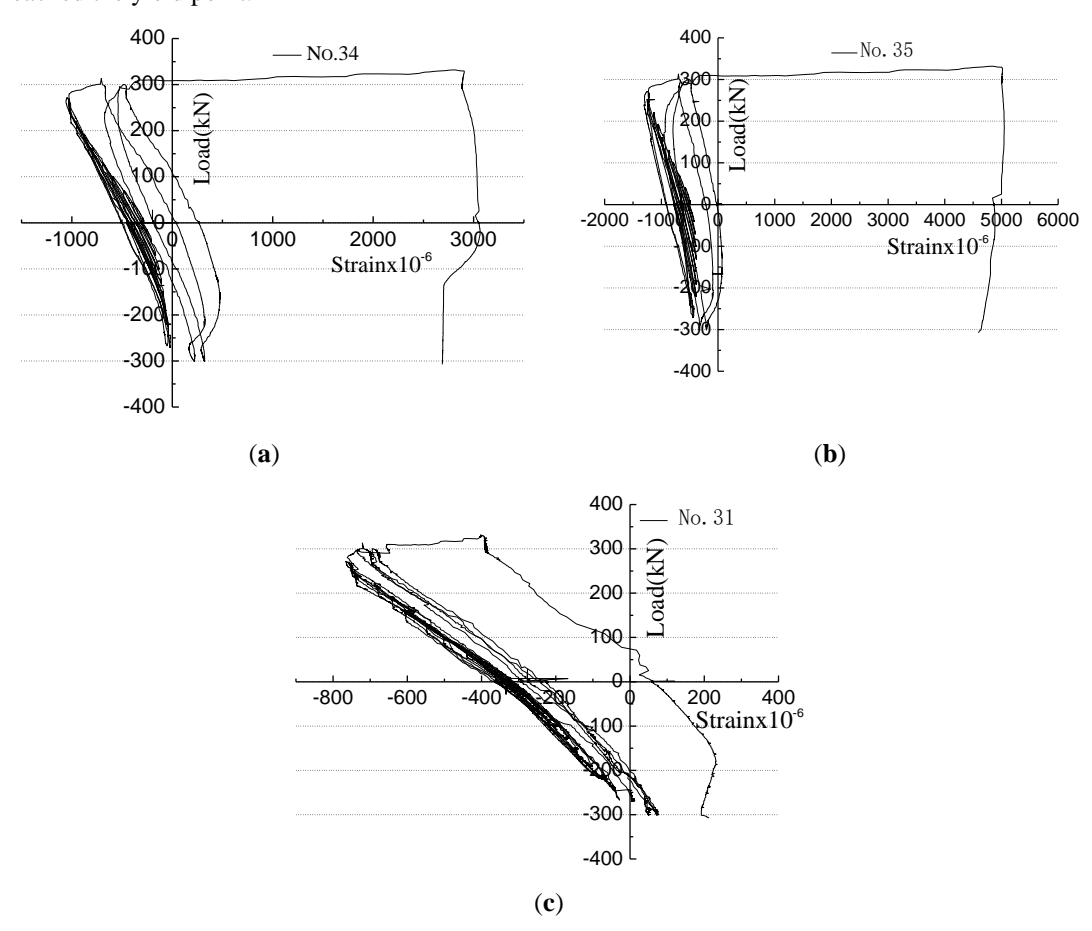


Figure 9. Load-strain curves of typical measurement points at the top flange of the column; (a) Measuring point S34; (b) Measuring point S35; (c) Measuring point S31

Figure 10 shows the load-strain curve of the typical measuring points of the lower column segment. The flange of the lower column is always in a compression state, and its general trend is consistent with that of the upper column, but the strain is far greater than that of the corresponding location of the upper column. The maximum strain of measuring point S36 is 7961.6×10⁻⁶, and measuring point S38 far from the flange of the joint remains in the elastic stage.

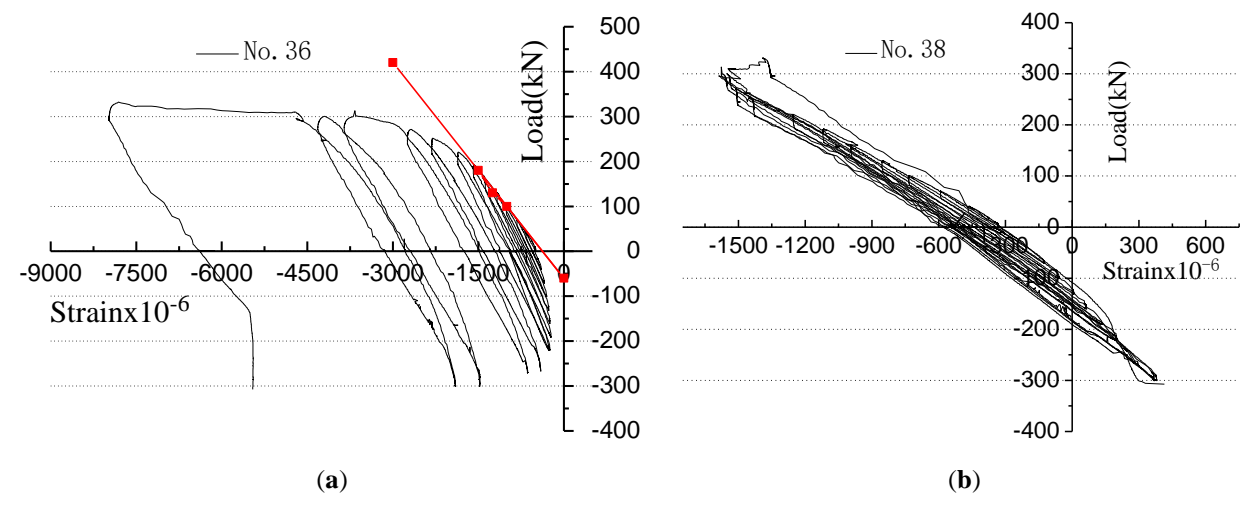


Figure 10. Load-strain curves of typical measuring points at the bottom flange of the column (a) Measuring point S36; (b) Measuring point S38

3.6 Strain intensity analysis of the supporting plate and its stiffened ribs

As an important component of the splice joint, supporting plates make it possible for the LHSB to connect the two segments by welding in the column web and flange. Due to the high pretension of the LHSB, the compressive stress concentration usually occurred around the bolt hole. To prevent the splice flange from local buckling, the stiffening plate was welded symmetrically under the supporting plates, forming a reasonable force transference path. Strain rosettes were arranged at the supporting plates and stiffened ribs near the welding line intersection, as shown in Figure 3. Figure 11 demonstrates the load-strain intensity curve of the measurement point; here, the strain intensity is defined as follows:

$$\varepsilon_{i} = \frac{\sqrt{2}}{3} \sqrt{(\varepsilon_{1} - \varepsilon_{2})^{2} + (\varepsilon_{2} - \varepsilon_{3})^{2} + (\varepsilon_{3} - \varepsilon_{1})^{2}}$$

$$\tag{4}$$

Where ε_1 , ε_2 , and ε_3 are the three-dimensional strain values measured from the strain rosette.

Figure 11(a) is the load strain curve of the supporting plate. (1) The strain of the supporting plate is very small, only 258.3×10⁻⁶, and the stress is 53.77 MPa, far less than the yield stress. The results show that the strengthening effect of the stiffened rib is significant; even though the supporting plate bears a large local preload, the strain remains small. The design of the supporting plate is reasonable, and the force transmission is efficient and reliable. (2) The strain of the upper column supporting plate is much larger than that of the lower column, and the strain value of the upper column supporting plate measuring point T1 is approximately 4.3 times that of the lower column supporting plate measuring point T19. The main reason for this difference is that the loading point is on the upper column, and under the cyclic load, the upper column displacement of the LHSB is larger, resulting in a greater stress at the supporting plate connected to it.

Figure 11(b) and Figure 11(c) show the load-strain curves of the upper and lower column stiffened ribs, respectively. The test points T3 (upper part) and T13 (lower part) near the intersection of the welds exhibit the maximum strains 1704.2×10⁻⁶ and 160.4×10⁻⁶, respectively, among the test points of the stiffened ribs, and the stress of the T3 test point is close to the yield limit. The strain values of T4, T5, T14 and T15, which are far from the intersection of the welds, are small, and the strain remains basically unchanged with increasing load. In general, the stiffened rib has an obvious stiffener effect, which effectively improves the bearing capacity and stiffness of the joint. At the same time, it provides a fixed support for the supporting plate and enhances its buckling resistance. The thickness of the supporting plate can be reduced due to the large stiffness in the stiffened rib. According to the test data, the supporting plate thickness of the test piece is slightly larger than necessary.

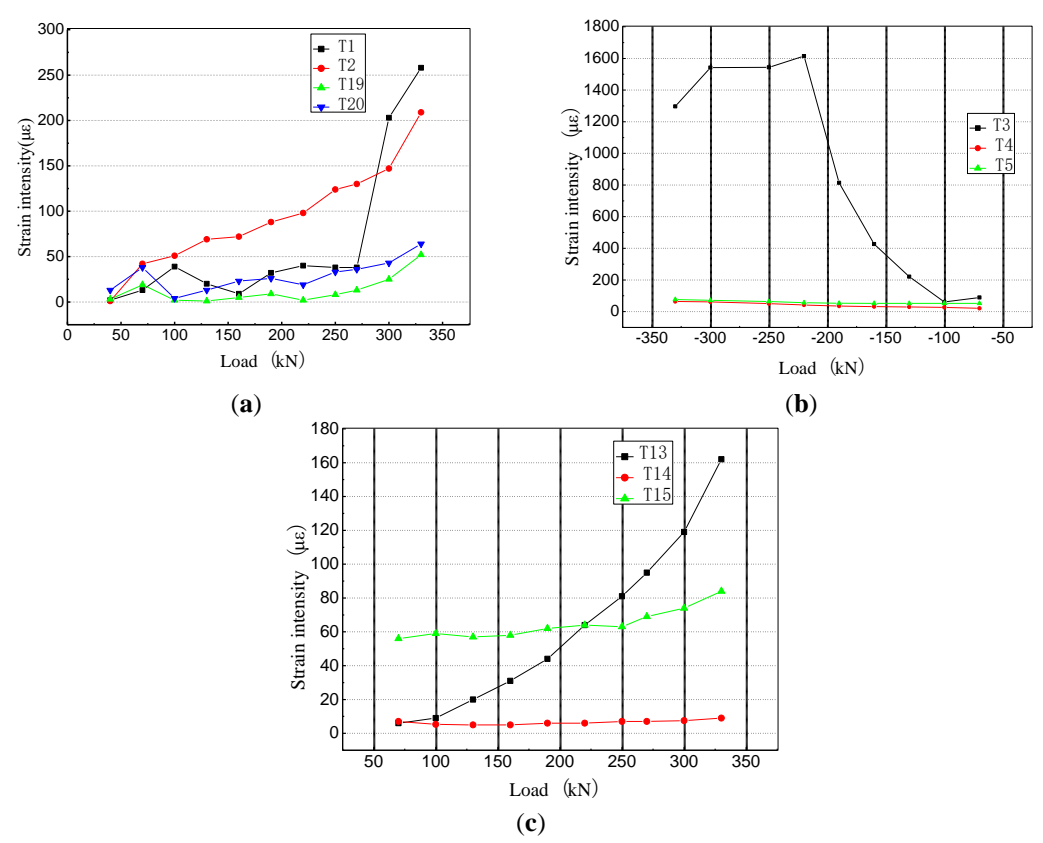


Figure 11. Load-strain curves of the supporting plate and stiffened rib; (a) Supporting plate; (b) Stiffenen rib at the upper segment; (c) Stiffenen rib at the bottom segment

3.7 Load-angle curve of the joint

The deformation of the joint core area is mainly shear deformation, which has an important influence on the study of the rotation capacity of the joint. Figure 3 demonstrates the test area for the shear deformation in the joint, as well as the layout of test points and measuring devices used during the test. In reference [27], the formula for calculating the shear angle of the joint area is given according to the deformation of the diagonal of the joint area in the test.

$$\gamma = \frac{\sqrt{h_{wc}^2 + h_{wb}^2}}{h_{wc}h_{wb}} \times \frac{\partial_6 - \partial_5}{2}$$
 (5)

where h_{wc} is the height of the joint zone; h_{wb} is the width of the joint zone; and δ_5 and δ_6 are the displacement values measured by displacement meters D5 and D6, respectively.

Figure 12 shows the load-shear angle curves of the three specimens. It can be seen from the figure that the shear angle increases slowly at the beginning of loading because the two columns are in close contact under the pretension of the LHSB. Due to the lack of experience in controlling pretension, the pretensioning of the high-strength bolt of specimen C1-1 caused it to exhibit a non-zero shear angle at the beginning of loading. During the first few loading cycles, the shear angles of the three specimens increase gradually. Figure 13 (b) shows that before the sharp increase in the shear angle, the maximum value of the shear angle is only 743.3×10⁻⁶ rad, indicating that the rotation stiffness of the spliced joint was large. When the load reachedapproximately 270 kN, the shear angle increased sharply due to the loss of the pretension of the longitudinal high-strength bolt and the loosening of the nut. The reason for the increase in the rotation angle is that the joint gradually loses the ability to transfer the horizontal shear force due to the flange separation of the two column segments. It can be seen from Figure 13 (c) that in the initial stage of loading, because the hinged end of the jack at the top of the column is not closely connected with the vertical reaction frame, the shear deformation angle increased sharply when the load reached approximately 200 kN. Due to the improper operation of the test, the ultimate load of test specimen C1-3 is only 198.2 kN.

It can be seen from the shear deformation angle curves of the three specimens that the maximum shear deformation angle of this spliced joint is 0.0023 rad, and the deformation is small. Therefore, the spliced joint is safe and effective.

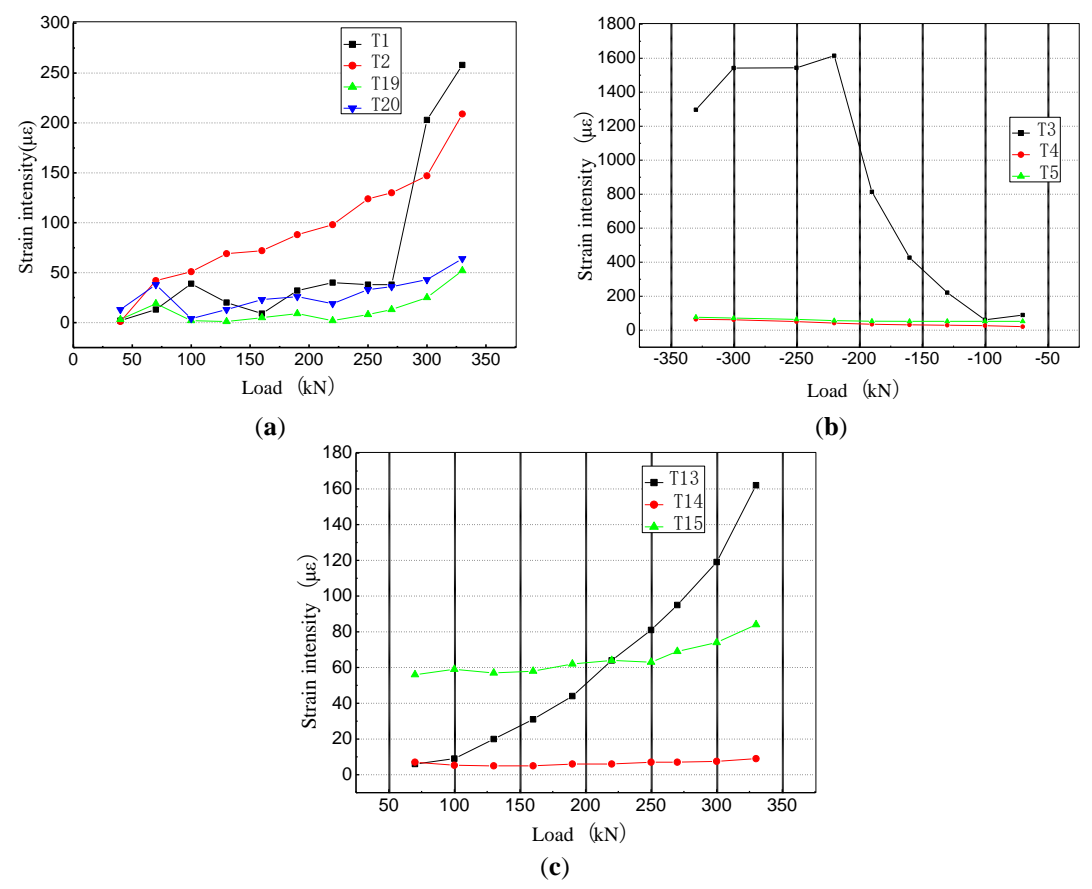


Figure 12. Load-rotational angle curves of the specimens; (a) Specimen C1-1; (b) Specimen C1-2; (c) Specimen C1-3

4. Corresponding Finite Element Model

To further understand the performance of the new spliced column joint, the FE program ANSYS was employed in three dimensions to replicate the moment-rotation behaviour and failure mode recorded in the tests of the connection. The finite element model representing the configuration of the test specimen is shown in Figure 13. Table 3 provides the finite element model labels and specifications.

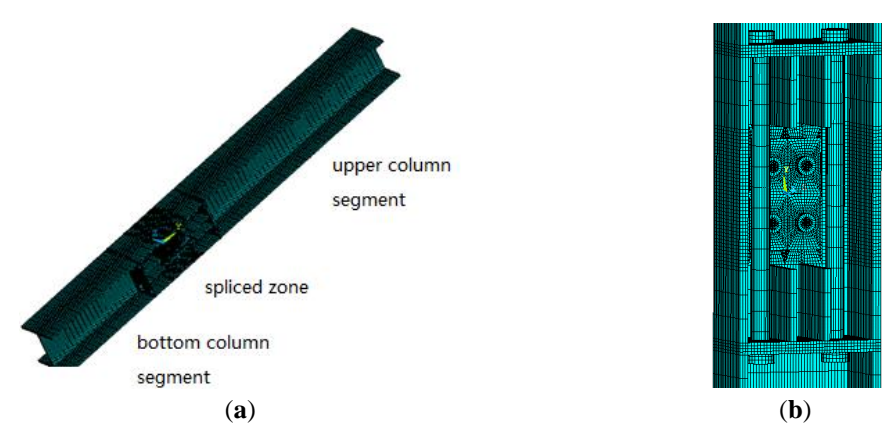


Figure 13. Mesh model of the joint (a) Overall finite element model; (b) Joint zone model

4.1 Material models

The stress-strain model obtained from tensile coupon test results of steel plates, represented by the trilinear stress-strain curve with strain hardening, is shown in Figure 14 and was used for the FE models. The plastic behaviour in the connection was represented by isotropic hardening and the von Mises yield criterion. The basic material properties of the plates are given in Table 1. The stress-strain curve of the high-strength bolt model adopted the three-fold line model proposed in reference [27], as

shown in Figure 15. In the figure, f_b^y and ε_b^y are the yield strength and yield strain of the high-strength bolt, f_b^u are the tensile strength and fracture strain of the high-strength bolt, and E is the elastic modulus of the high-strength bolt material. The material properties of the bolt are determined according to the test. The yield strength and tensile strength of Grade 8.8 M20 high-strength bolts are 768 N/mm² and 966 N/mm², respectively. The actual yield strength and tensile strength of the Grade 10.9 M30 were 1079 N/mm² and 1205 N/mm², respectively.

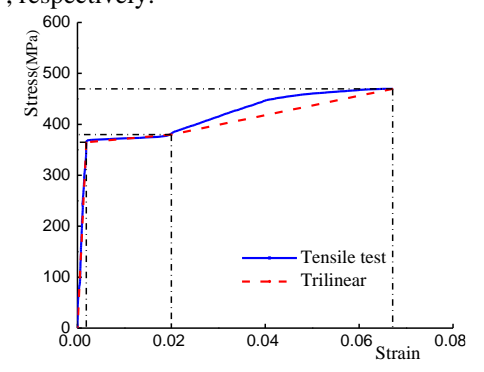


Figure 14. Stress-strain curves for the FE model

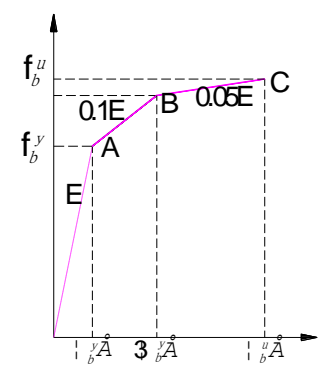


Figure 15. The trilinear curve of the high-strength bolt for the FE model

4.2 Finite element model description

In this model, the elements used are all chosen from those available in ANSYS. All the components are modelled using the solid element Solid185, defined by an 8-node brick with full integration. The Prets179 element is used to provide bolt pretension. In the model, many contact regions are taken into consideration.

The initial geometric defects of the steel columns in the finite element model are not considered, that is, the effects of the initial bending and torsion of the steel columns are not considered, and the cold working effect and welding residual stress of the steel plates are ignored to simplify the joint model.

Displacement control loading was adopted in this calculation, and the loading point was located one metre from the spliced point. There are three analysis steps in the calculation process: the first step is to apply pretension to the LHSB, the second step is to apply axial pressure to the steel column, and the third step is to exert a cyclic load to the spliced joint of the steel column, as shown in Figure 16.

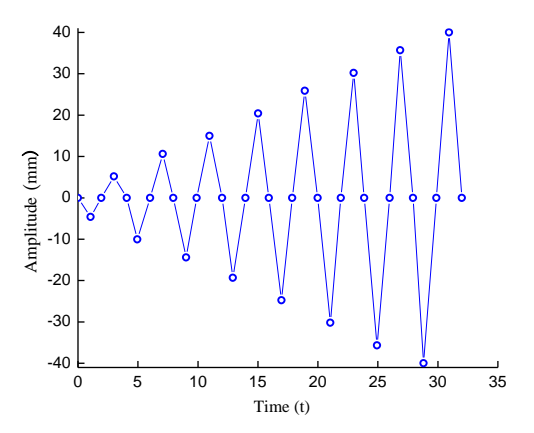


Figure 16. Cyclic loading protocol

To prevent rigid displacement occurring before the contact relation was established in various parts, an extra analysis substep and boundary condition were applied. Specifically, the temporary constraint was applied at the bottom flange, and then the load was gradually exerted on the model. As a result, the model smoothly enters the contact state and then eliminates the temporary constraints. The method mentioned above effectively avoids the divergence problem due to the large rigid displacement.

The contact element was covered in the contact region of the FE model. The deformation between the two supporting plates as well as bolt slippage were the key analysis points, so the face-to-face contact must be considered, and six contact pairs were defined: 1. bolt head and flange plate; 2. bolt nut and flange plate; 3. two flange plates; 4. bolt shank and hole of the flange plate; 5. bolt head and splice plate of the beam web; and 6. splice plate and web of the beam. The augmented Lagrangian method was used to solve the equations. When two surfaces had friction, the penalty method was implemented. The frictional coefficient of the steel plate was taken as 0.4 without considering the initial penetration. The contact properties were adjusted to obtain a smooth solution and to avoid over-closures and inter-penetrations of the contacting parts.

Both material and geometric nonlinearities were considered to predict the moment-rotation curve, ultimate bearing capacity, etc. The Newton-Raphson incremental interaction method and contact algorithm penalty function were used in the solution. A convergence criterion was set to 0.4% for force or moment checking, and the normal penalty stiffness factor value varied from 1.0 to 1.5 according to the different load cases.

4.3 Results and discussion of the monotonic load case

4.3.1. Calibration of the FE model

The predicted failure mode of specimens C1-1 under cyclic loading is illustrated in Figure 17, and the deformation characteristics of the steel column splice joints in different stages are shown in Figure 18. It can be seen from the figures that the finite element model accurately simulates the whole process of the test component from the flange buckling to the whole failure. The deformation of the column connection region and buckling of the column stiffening rib were consistent with the test results.

The failure of the specimen is due to the local buckling deformation of the flange at the column connection area, which leads to the staggered edge of the upper and lower columns. The finite element model can accurately simulate this phenomenon observed

during the experiment. With the increase in load, the displacement at the top of the column increases, and with the loosening of the LHSB, the spliced column segment no longer remains vertical, so that the flange at the connection of the upper column separates from the lower flange. In the test, the LHSB did not deform, but the finite element results show that the screw bent. The reason is that contact between the supporting plate and the nut of the LHSB was set as a binding contact. Although the contact can be set as standard contact, this will cause the calculated ultimate load to be too large and make convergence difficult. When the model utilized a binding contact, the load-displacement curve was in good agreement with the test result, so the final model utilized a binding contact.

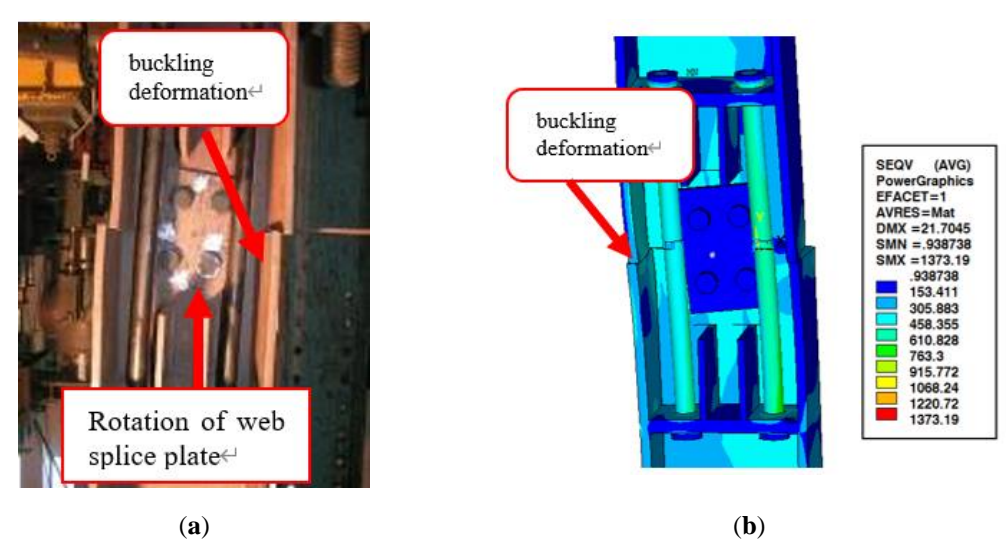


Figure 17. Oserved and predicted failure modes at ultimate load(a) Test model; (b) FEA mode

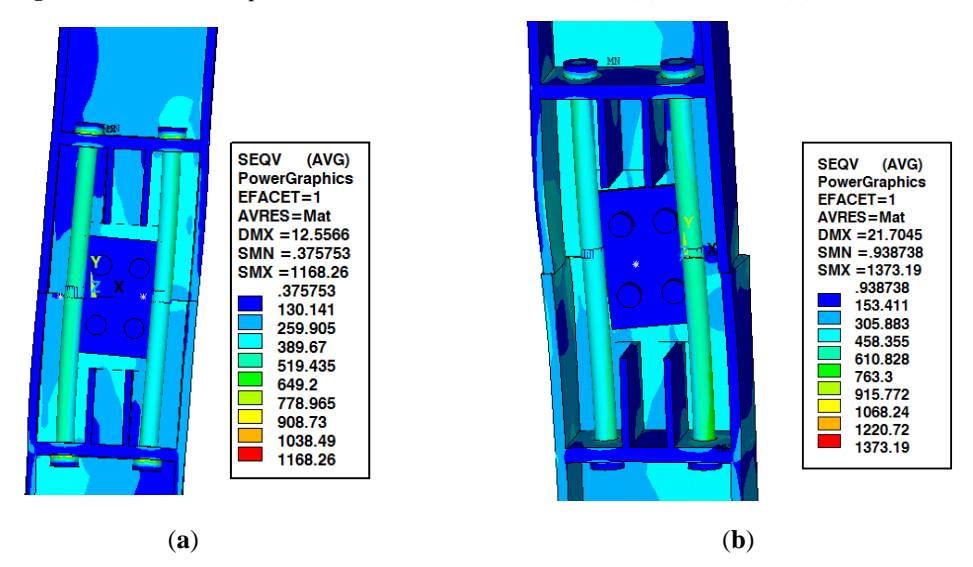


Figure 18. Deformation and stress of the joint in different loading phases (a) Elastic stage; (b) Plastic stage

4.3.2 Hysteresis curves

The comparison between the hysteresis curve calculated by the finite element model and the test results is shown in Figure 19. The hysteresis curve calculated by ANSYS is in good agreement with the test curve in the elastic stage, but the plastic stage, final failure and unloading process calculated by the model are different from the test results. This is related to the accuracy of the finite element simulation of the looseness of the LHSB because the simulation process of the bolt is relatively complex, and whether the applied prestressed value reached the expected value and the prestress lost were uncertain when the prestress was applied in the test. However, the finite element model was relatively idealized, which led to a deviation in the final failure mode between the finite element calculation result and the test result.

Figure 19 shows that the ultimate load is 351.2 kN, and the deviation between the finite element calculation result and the test result is very small. However, the initial stiffness results are not completely consistent: the finite element value is 16..88 kN, and

the test result is 12. 1 kN/mm. In general, the finite element numerical simulation method, the selected material parameters and the constitutive model can be used to simulate the actual stress state of the test component.

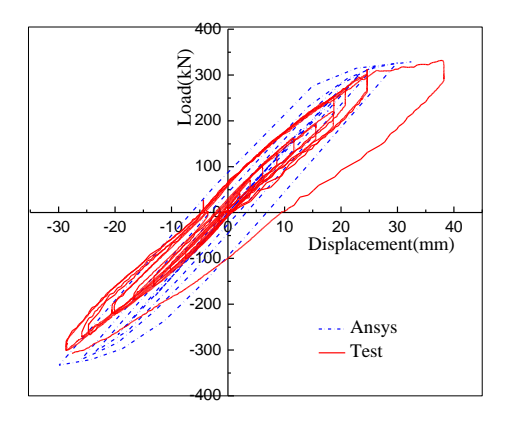


Figure 19. Hysteresis curves

4.3.3 Stress distribution of the supporting plate and LHSB

The supporting plate, as an important component of the column spliced joint, guarantees the effective connection of the pretensioned LHSB. The stress distribution characteristics of the supporting plate and LHSB are shown in Figure 20. It can be seen from the figure that after the pretension and horizontal cyclic loading of the prestress are applied, the area with a high stress is mainly concentrated near the edge of the bolt hole and the connection between the flange plate and stiffening plate. Since the stress diffusion of the gasket was not considered in the modelling, the stress concentrates near the bolt hole, and the maximum value is 350 MPa. Due to the small number of strain gauges arranged on the flange plate in the test, it is not meaningful to compare the finite element calculation results and test results, so no comparative analysis of the two stress results is provided, but the finite element analysis can accurately simulate the stress distribution characteristics of the flange plate.

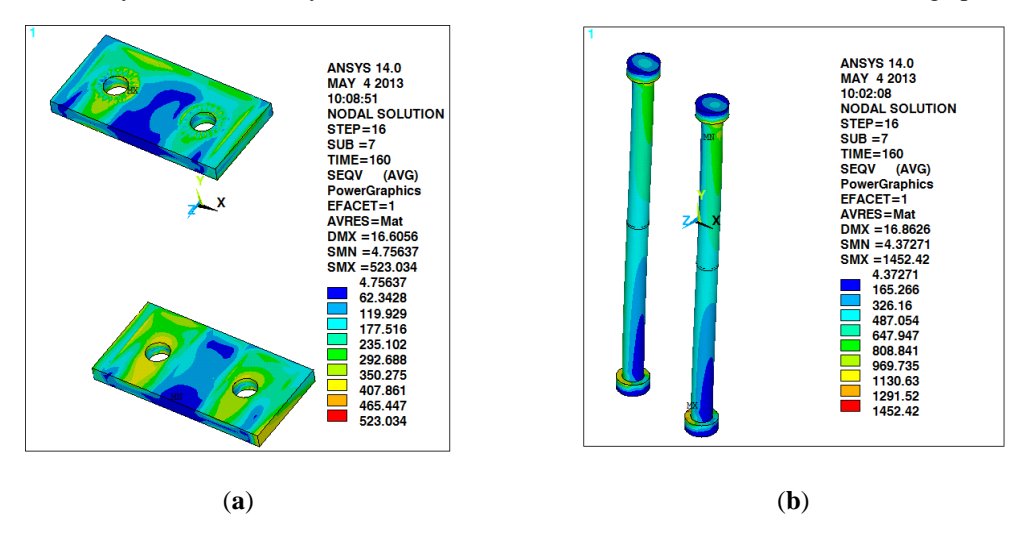


Figure 20. Stress distribution of the supporting plate and LHSBs in the ultimate load(a) Supporting plate; (b) LHSB

Although the first buckling deformation occurs at the column flange, the joint was not destroyed immediately. With increasing load, the connection effect of the prestressed longitudinal high-strength bolt was very significant. Figure 20 shows the von Mises stress distribution of the LHSB under ultimate load. It can be seen from the figure that the maximum stress of the LHSB occurs at the nut, which is connected to the supporting plate; the maximum stress is 815.17 MPa. The LHSB is in the elastic stage and does not reach the yield stress. According to the result of the stress distribution, the axial force can be obtained.

Table 2 shows the comparison between the von Mises stress of the FEM and the test result in the elastic stage. The value in the table is the stress of the measuring point under the previous level load when the measuring point enters the plastic stage. In this stage, the horizontal jack load is 270 kN, the stress value is the average value of the test results of the three specimens, and the finite element stress value is the calculated value under the same load as the test. In the table, $Error = (finite element calculation-value test value) \times 100\% / test value. It can be seen from Table 2 that the calculated stress magnitude of the finite element of the$

left LHSB is too high, which is quite different from the test result, but the stress result of the right LHSB is basically consistent with the test result. The reason for these differences is that the finite element model was more ideal, and the model did not consider the influence of the initial geometric defects of the steel structure. Furthermore, there are many uncontrollable factors in the experiment, so measurement error is inevitable.

Table 2. Comparison of the von Mises stress between the FEM and test results in the elastic stage of the LHSB (MPa)

Strain gauge Number		S1	S2	S3	S4	S5	S6	S7
Left	Test results	25.71	12.85	19.27	32.95	17.68	16.88	17.28
side	Calculated value	42.3	20.3	20.4	25.3	26.1	29.8	32.1
	Error	64.6%	57.9%	5.8%	23.2%	47.6%	76.5%	85.7%
Right side	Test results	175.1	169.2	174.3	176.2	180.7	180.2	180.3
	Calculated value	195.3	187.3	186.3	182.8	174.1	170.5	190.6
	Error	11.5%	10.7%	6.8%	3.75%	3.65%	5.5%	5.7%

4.3.4 Stress distribution of the high-strength bolt of the column web

The high-strength bolt of the web plate mainlyresists shear. Figure. 21 shows the von Mises stress distribution of the M20 bolt at the web under the ultimate load. It can be seen from the figure that the von Mises stress is not uniformly distributed in the bolt after the pretension is applied to the bolt, but the stress distribution in the middle of the bolt bar is basically uniform. However, near the bolt head and nut, the stress is higher, and the maximum value can reach 239.112 MPa. Due to the small internal force at the splicing point, the maximum stress is 31% of the elastic limit of the bolt material, which can be properly adjusted in the design to reduce the cost of construction.

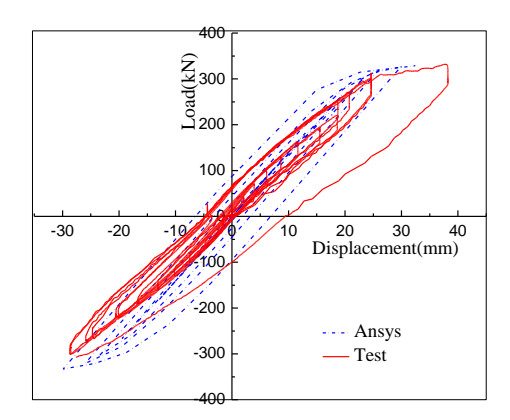


Figure 21. Stress distribution of the high-strength bolt of the column web

5. Parameter Studies

In the experimental programme, only limited dimensions and material strengths of the joint were considered. To shed light on the effects of the diameter of the LHSB, the size of the web plate, the number of web bolts, the thickness of the splice flange plate, and the height of the steel column section, a series of parametric studies were conducted based on the validated numerical model. In addition, the axial force of the column and the pretension of the LHSB of the spliced joint also have a certain impact on the moment rotation characteristics of this new joint, so the changes in these two parameters are also studied.

5.1 Diameter of LHSB and height of column cross-section

By varying the diameter of the LHSB and the column section height, twenty joints were designed to study the influence of the two parameters on the spliced joint stiffness and ultimate bending moment. Figure 22 shows the M- ϕ curve of the joint with different bolt diameters and column section sizes. The numerical results show that when the column section is small, the bolt has little effect on the initial stiffness of the joint, but the ultimate bending moment increases with increasing bolt diameter. When the column section height is greater than 400 mm, the initial stiffness and ultimate moment of the column increase greatly. The

maximum value of the rotational rigidity is 94240 kN.m/rad, and the maximum value of the ultimate bending moment is 652 kN.m at joints with section heights equal to 600 mm and bolt diameters of 30 mm. However, the angle corresponding to the ultimate moment decreases with increasing column height. As an important connection component of a spliced joint, the LHSB has a great influence on the stiffness and ultimate moment of the joint. When the diameter of the high-strength bolt reaches M30, the ultimate moment is 2-3 times higher than that of the M20 connection.

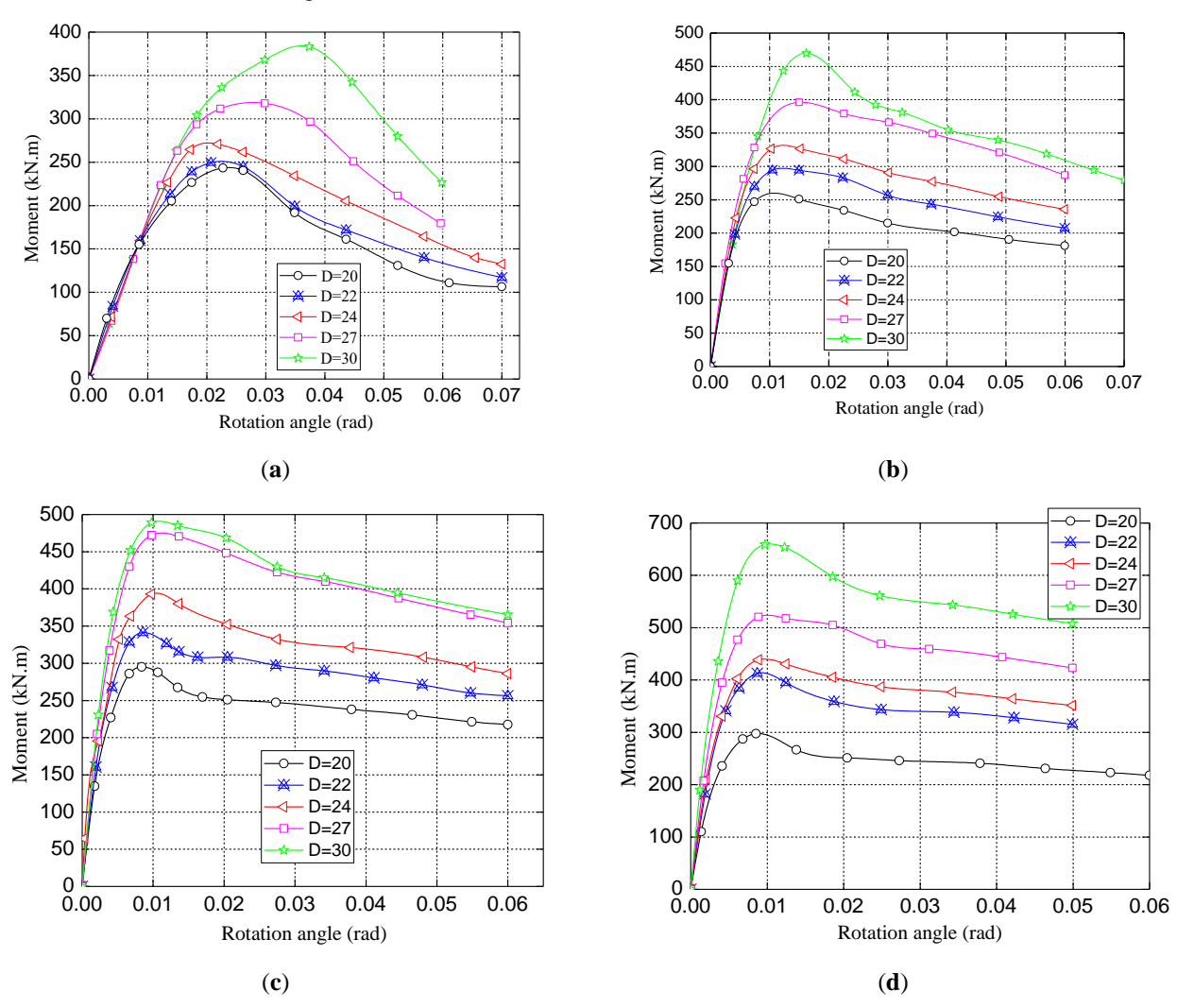


Figure 22. $M-\varphi$ curves for various parameter Hw and D values (a) Hw=250 mm; (b) Hw=400 mm; (c) Hw=550 mm; (d) Hw=600 mm

5.2 Influence of β

The failure of the column joint began with the local buckling of the column flange, which led to the dislocation of the two column segments. Therefore, the ratio of the extended width of the steel column flange plate to its thickness is an important factor and is defined as β . According to the section of the I-shaped column commonly used in actual projects, β was taken as 12, 11, 10, 9, and 8.6, the column section was selected as 250 mm, 400 mm, 550 mm, and 600 mm, while the other geometric parameters remained unchanged.

Figure 23 shows the M- φ curves with changing parameters β and Hw. The numerical results show that by increasing β of the joint from 8.6 to 12, the ultimate bending moment and initial stiffness are substantially decreased when the column section height is less than 400 mm, as shown in Figure 23(a). It can also be seen from Figure 23(a) that the initial stiffness reaches the maximum value of 17667 kN·m/rad and the ultimate moment is 382 kN·m when β is equal to 8.6. When the column section height equals 400 mm, the ultimate moment does not change considerably, but when β is equal to 12, the bending moment decreases rapidly with increasing rotation angle, as shown in Figure 23(b). Figure 23 (c)-(d) shows almost no obvious change in the ultimate bending moment and initial stiffness. The results of the finite element analysis also show that the failure of the column is no

longer the local buckling of the column flange at the joint area but the prestress relaxation of the LHSB. Therefore, when the column section is small, it is necessary to add structural measures to prevent local buckling of the flange.

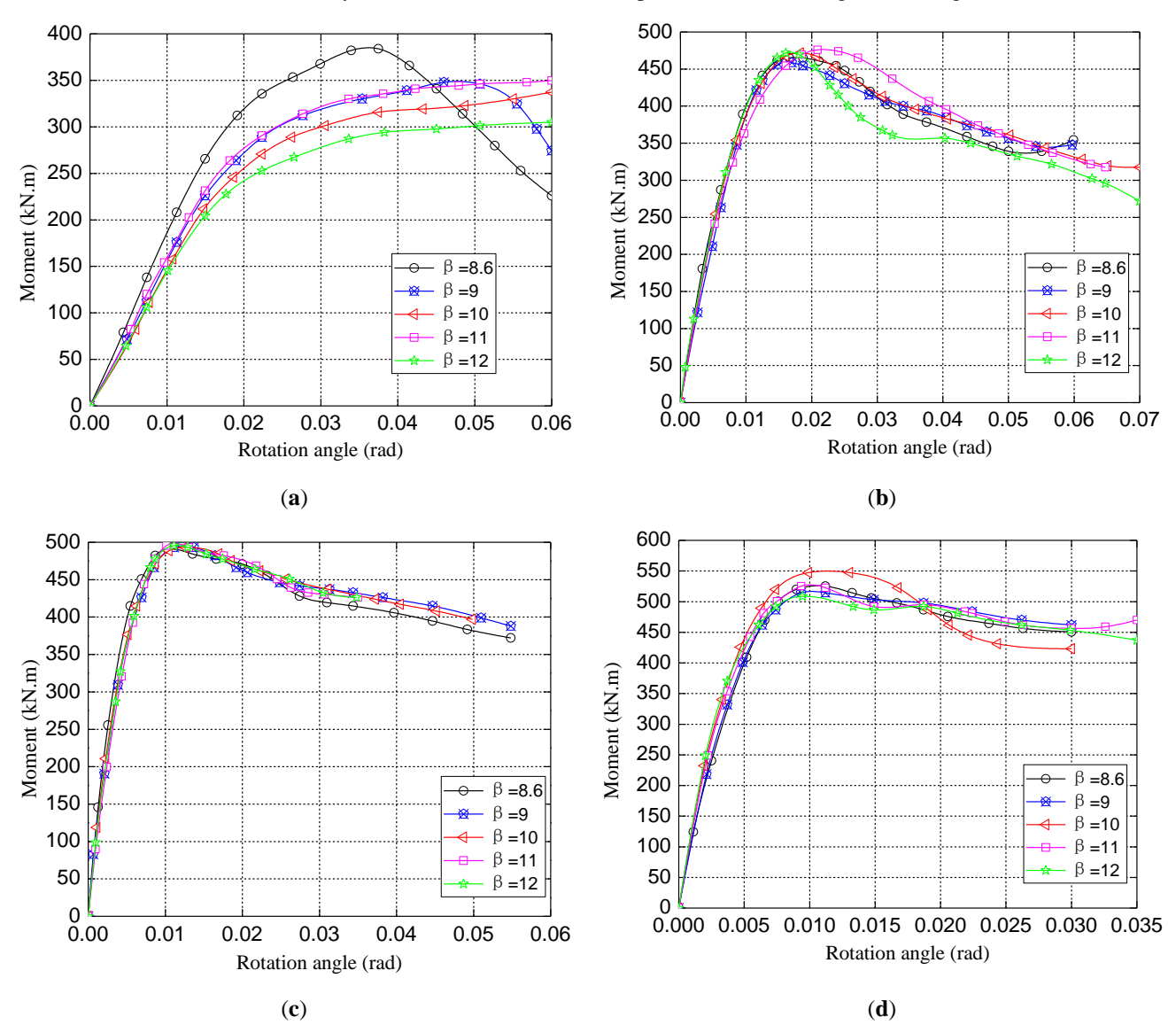


Figure 23. $M-\varphi$ curves for various parameter Hw and β values (a) Hw=250 mm; (b) Hw=400 mm; (c) Hw=550 mm; (d) Hw=600 mm

5.3 Effect of different pretensions

It is necessary to investigate the reduction in the ultimate bending moment under different pretensions because of the inevitable loss of pretension. Figure 24 shows the M-φ curve under different pretensions (0.2P, 0.4P, 0.6P, 0.8P, and 1.0P), respectively. It can be seen from Figure 24 that the ultimate bending moment is reduced by 15.8% when the applied pretension is 0.8P and 24.5% when the applied pretension is 0.6P. However, the reduction in pretension has little effect on the initial stiffness, which remains at approximately 18000 kN·m/rad. In addition, the difference in the limit rotation angle also varies greatly with different pretensions, and the limit angle can reach 45.2 mrad when the pretension equals 1.0P. Therefore, the steel column splice joint with no loss of pretension performs well, so the exertion of pretension is an important control factor of splice joint construction.

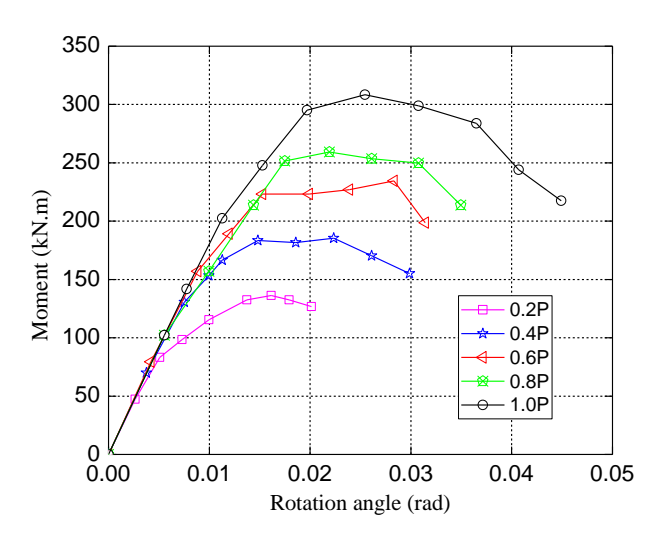


Figure 24. M- ϕ curves for different bolt prestresses

In view of the important influence of pretension on the performance of steel column spliced joints, the hysteresis performance of steel column spliced joints under different pretensions is shown in Figure 25, and a supplementary analysis of the pretension effect is carried out. Numerical results show that the ultimate displacement and load increase significantly with increasing pretension. When the pretension is equal to 1.0P, the ultimate lateral displacement reaches the maximum value of 30 mm. When the pretension is greater than 0.6P, the ultimate load changes only slightly. The pretension plays a key role in the stiffness continuity and mechanical properties of the joint.

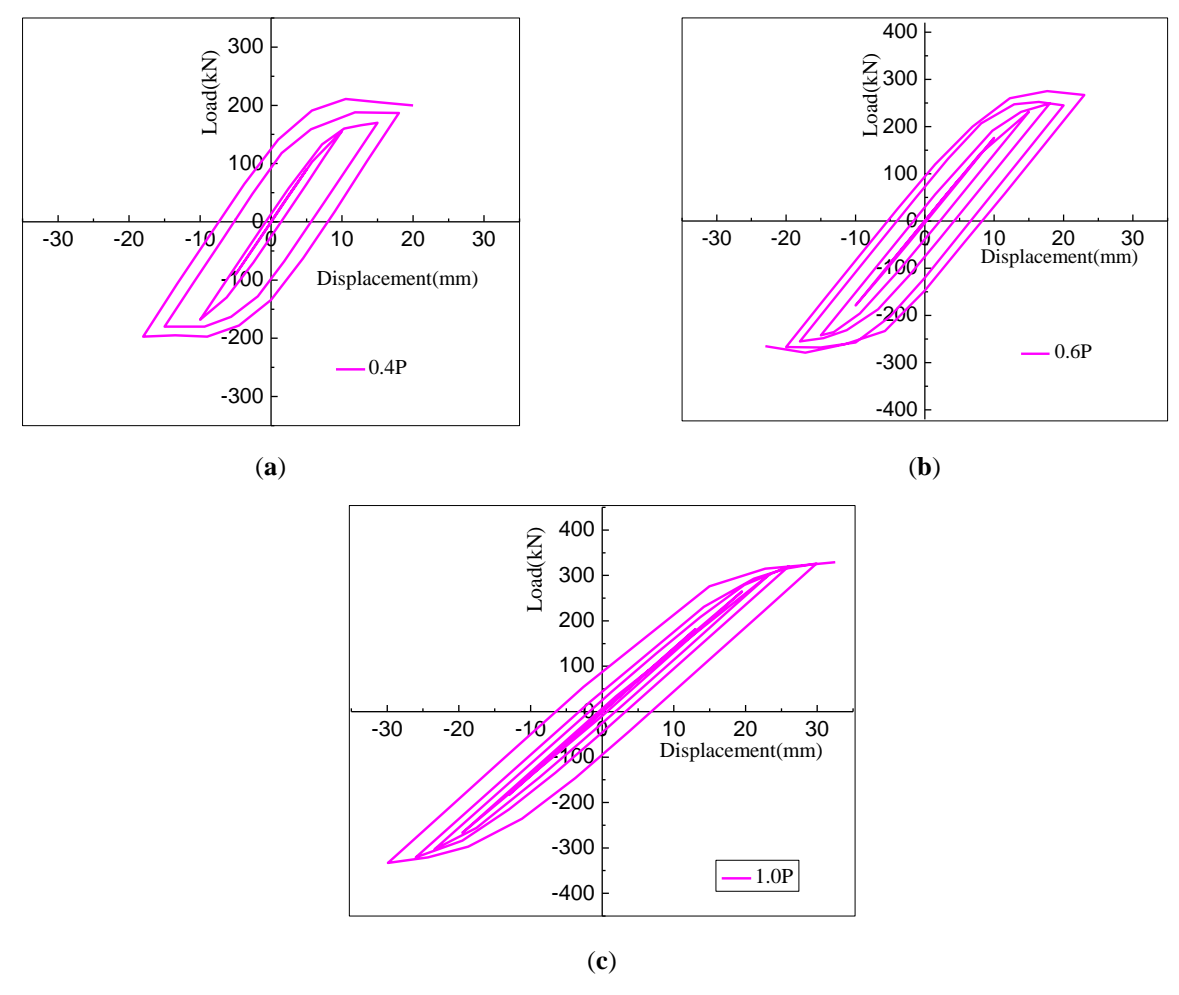


Figure 25. Hysteresis curves of different prestresses

6. Conclusions

This paper studied a new type of spliced column-to-column joint, called pretensioned moment-resistant joint. A total of 3 specimens were designed and tested under cyclic loads with axial compression of the columns. A FE model of the tested specimens was also developed. In addition, parametric studies were carried out based on the validated model, and the following conclusions were drawn from the numerical simulations. The failure mode, resistance, stiffness and ductility of the specimens were analysed, and the main conclusions are as follows.

- (1) The longitudinal high-strength bolt plays an important role in the connection of the joint, and it is the critical component for the joint to be successfully spliced to ensure its strength and maintain its ability to transfer axial forces, shear forces and moments. The test results show that the longitudinal high-strength bolt remained in the elastic stage, and its deformation was very small under the condition of axial compression on the top of the column. The two parts of the column were closely connected, and the bolt holes in the supporting plate welded at the web plate exhibited no slip damage. Therefore, bolts with a larger diameter and strength of no less than Grade 10.9 were selected to apply a larger pretension and present a strong connection effect on the two parts of the columns, which is the core design idea of this column-to-column spliced joint.
- (2) The supporting plate is also an important component of this pretensioned moment-resistant joint. The supporting plate ensures that LHSB is pretensioned. The pretension will produce a large pressure on the supporting plate. If the flange plate is thin, buckling deformation will occur under the cyclic load. In addition, the stiffeners symmetrically welded at the supporting plate have an obvious stiffening effect, which can effectively prevent the buckling deformation of the supporting plate and indirectly ensure the splicing of the two column parts.
- (3) The failure of the joint was divided into two stages. The first was the column flange buckling deformation, which weakened the milling of the flange section and caused serious misalignment. However, at this time, the second line of defence was the LHSB, so the joint continued to bear the load. When the bearing capacity was lost, the LHSB was far from yielding. Due to the use of a LHSB, and the supporting plate and stiffener rib are welded in a factory, the field operation is simplified, and the quality is easier to ensure.
- (4) The finite element model of the joint can simulate the hysteresis performance and deformation mode of the column flange after buckling deformation. The hysteresis curve of the new joint under cyclic loading is in good agreement with the test, and the bearing capacity under large deformation is close to the test results, but the lateral displacement of the loading point during failure is obviously larger. Because the performance of the joint depends on the high-strength bolt with high pretension, the loss of pretension will be important. The pretension value has a great influence on the joint performance. When the pretension is applied at 0.8P, the ultimate moment can be reduced by 15.8%, while when the pretension is applied at 0.6P, the ultimate moment can be reduced by 24.5%. However, the reduction in pretension has little effect on the initial stiffness, which remains at approximately 18000 kN·m/rad. The ratio β , the extension width of the steel column flange plate to its thickness, also has a great influence on the joint performance. When this ratio is large, the flange at the column splicing joint is prone to local instability, thus accelerating the failure of the joint, which shows that the ultimate moment is small, and the ultimate moment decreases with the increase in β . The key factor in the design of steel column prestressed flexural joints is to choose the ratio of the width of the column flange to its thickness to delay the local instability of the column flange.

Author Contributions: This paper was independently completed by Yufeng Jiao.

Funding: This research received no external funding.

Data Availability Statement: The datasets used and/or analyzed during the current study are available from the corresponding author on reasonable request.

Acknowledgments: I would like to express our gratitude to the Structural Laboratory of Henan University of Science and Technology for their support in the experiment.

Conflicts of Interest: The author declare no conflicts of interest.

References

- [1] GB/T 50378, Assessment Standard for Green Building, China Building Industry Press, Beijing, China, 2013 (in Chinese).
- [2] Y.Y. Chen, Y.C. Yu, Floor-by-floor assembled steel braced structures for prefabricated buildings, *Build. Struct* **2012**,10,48–52 (In Chinese).

- [3] L. Jaillon, C.S. Poon, The evolution of prefabricated residential building systems in Hong Kong: a review of the public and the private sector, *Autom. Constr*, 2009, 18 (3), 239-248.
- [4] T.N. Dao, J.W. van de Lindt, Seismic performance of an innovative light-frame cold-formed steel frame for midrise construction, *J. Struct. Eng*, 2013, 139,837–848.
- [5] Serrette, R. Seismic design strength of cold-formed steel framed shear walls, *J Struct Eng*, 2010, 136(9), 1123-1130.
- [6] CHEN Yueshi, WANG Wei, CHEN Yiyi. Full-scale shaking table test of a three-story floor-by-floor assembled steel braced frame. *Build. Struct*, 2018, 39(9), 22-29(in Chinese)
- [7] ZHANG Yanxia, ZHANG Ailin, SUN Wenlong. Behavior study of self-centering beam-column connections in resilient steel frames after earthquake. *Industrial Construction*, 2014,44(11),160-167
- [8] X.C. Liu, A.X. Xu, A.L. Zhang, Z. Ni, H.X. Wang, L. Wu, Static and seismic experiment for welded joints inmodularized prefabricated steel structure, *J. Constr. Steel Res*, 2015, 19 (9) ,183–195.
- [9] X.C. Liu, S.H. Pu, A.L. Zhang, A.X. Xu, Z. Ni, Y. Sun, L. Ma, Static and seismic experiment for bolted-welded joint in modularized prefabricated steel structure, *J. Constr. Steel Res*, 2015, 115, 417-433.
- [10] Snijder H.H., Hoenderkamp JCD. Influence of end plate splices on the load carrying capacity of column. *J Constr Steel Res*, 2008, 64(7-8), 845-853.
- [11] Ana M.Giral Coelho, Pedro D.Sima, Frans S.K.Bijkaard. Stability design criteria for steel column splices, *J Constr Steel Res*, 2010,66(10),1261-1277.
- [12] PD Simão, AM Girão Coelho, FSK Bijlaard. Influence of splices on the buckling of columns, Int J Nonlin Mech ,2012,47(7),806-822.
- [13] J. Shen, T. Sabol, Seismic demand on the column splices in special steel moment frames, in: Technical Report to American Institute of Steel Construction, American Institute of Steel Construction, Chicago, IL, 2008.
- [14] AISC 341. Seismic provisions for steel structural buildings, AISC 341-10. Chicago, IL: American Institute of Steel Construction; 2010.
- [15] Bulent Akbas, Jay Shen, Thomas A. Sabol. Estimation of seismic-induced demands on column splices with a neural network model, *Appl Soft Comput*, 2011(11), 4820-4829
- [16] Bulent Akbas, Bilge Doran, Thomas A.Sabol. Effect of various span lengths on seismic demand on column splices in steel moment frames, Eng Struct, 2014, 70, 94-105
- [17] C.C.Baniotopoulos. Sensitivity analysis results on the separation problem of bolted steel column-to-column connectons, *Int J Solids Struct*, 1995, 32(2), 251-265.
- [18] J.Lindner.Old and new solution for contact splices in column, J Constr Steel Res, 2008,64,833-844.
- [19] H.C. Cui, A review of the damage caused by the earthquake that occurred in the south of Hyogo Prefecture in Japan, *J. Build. Struct.*,1996,17 (1),2–13(In Chinese).
- [20] M.D. Engelhard, T.A. Sabol, Seismic-resistant steel moment connections: development since the 1994 Northridge earth-quake, Prog. *Struct. Eng. Mater.*, 1997,I (I),68–77.
- [21] Kimberly Stillmaker, Xai Lao, Carmine Galasso, Amit Kanvinde. Column splice fracture effects on the seismic performance of steel moment frames, *J Constr Steel Res*, 2017,137,93-101
- [22] C. Galasso, K. Stillmaker, C. Eltit, A.M. Kanvinde, Probabilistic demand and fragility assessment of welded column splices in steel moment frames, *Earthq. Eng. Struct. Dyn.*, 2015, 44
- [23] Y.Q. Wang, L.Zong, Y.J.Shi.Bending behavior and design model of bolted flange-plate connection, *J Constr Steel Res*, 2013,84,1-16
- [24] Bartlomiej Blachowski, Witold Gutkowski. Effect of damaged circular flange-bolted connections on behaviour of tall towers, modelled by multilevel substructuring, *Eng Struct*, 2016, 111,93-103
- [25] X.C.Liu, X.N.He, H.X.Wang, Z.W.Yang, S.H.Pu, Zhang Ailin.Bending-shear performance of column-to-column bolted-flange connections in prefabricated multi-high-rise steel structures, *J Constr Steel Res*, 2018, 145, 28-48
- [26] GB50017-2017, Standard for Design of Steel Structure, China Architecture & Building Press, 2017(In Chinese).
- [27] Shi Yundong. Experimental study on seismic behavior of light steel structure joints of portal steel frame ,Shanghai,Tongji University,2009,P22.
- [28] A. N. Sherbourne, M. B. Bahaari. 3D simulation of end-plate bolted connections, J Struct Eng, 1994, 120(11),3122-3126